Centralized Photovoltaic Heliostat Field Layout and Optical Perception Optimization Based on Improved Dung Beetle Optimization Algorithm

Bin Liu[1,2], Chengyu Jiang[3,5*], Biguang Kong[1], Jiayu Wu[4,5], Junwei Yang[5]

[1]Nujiang Power Supply Bureau, Yunnan Power Grid Co., Ltd, Kunming, China

[2]Yunnan Power Grid Company Market Department, Yunnan Power Grid Co., Ltd, Kunming, China

[3]Faculty of Civil Aviation and Aeronautical, Kunming University of Science & Technology, Kunming, China

[4]Faculty of Transportation Engineering, Kunming University of Science & Technology, Kunming, China

[5]Longshine Technology Group Co., Ltd, Wuxi, China

Abstract

The gradual depletion of fossil fuels underscores the pressing need for technological advancements in renewable energy. These technologies are essential to address the inefficiencies in power generation from heliostat fields. This paper proposes an innovative heliostat field layout model aimed at significantly enhancing the efficiency of photovoltaic power generation. By carefully optimizing the positioning, height, and size of the heliostats, the model results in a substantial increase in annual heat output. Additionally, an improved Dung Beetle optimization algorithm (RCDBO) is introduced, which integrates random walk and cross strategy to enhance solving efficiency and accuracy while effectively avoiding premature convergence. Simulations demonstrate that the proposed algorithm achieves a 3% increase in efficiency compared to the traditional DBO algorithm, confirming the superiority of the RCDBO algorithm.

Keywords: heliostat field, dung beetle optimization algorithm, crossover strategy, random walk strategy

1. Introduction

In recent years, energy production from fossil fuels has increased greenhouse gas (GHG) emissions, contributing to climate change in some developed and developing countries [1]. To reduce the reliance on fossil fuels, countries are actively developing renewable energy sources [1-2]. Solar energy, as a paradigm of sustainable development and green energy, is increasingly receiving widespread attention and favor around the globe due to its abundant energy reserves and clean, non-polluting characteristics [3]. In solar tower power plants, the heliostat mirror field accounts for 50% of the total cost and causes 40% of the power loss [4]. Mirror layout is one of the critical factors in determining the energy harvesting efficiency and price of a heliostat system. In tower PV power plants, the construction cost of the heliostat mirror field accounts for 30% to 50% of the total investment [5]. Therefore, optimizing the layout of the heliostat mirror field is very important to improve the energy harvesting efficiency. However, many of these studies still need to work on the inefficiency problem [6].

Numerous scholars have integrated heliostat field planning with various innovative algorithmic models to design a more scientifically sound and reasonable mirror field. Based on this integration, they have proposed diverse arrangement methods for heliostat fields suited to different scenarios. Concerning model development, Atif et al. [7] formulated a mathematical model and employed differential evolution to conduct annual finite optimization of the heliostat field. Zou et al. [8] focused on optimizing the layout of solar mirror arrays using the Niching and Elite Competition Swarm Optimization (NECSO)

* Corresponding author. E-mail address: 15559937227@163.com

English language proofreader: Yen-Chun Hsieh

algorithm. This study introduces the competitive mechanism and efficacy of the NECSO algorithm, contrasting its performance against seven other algorithms. Experimental results demonstrate that NECSO excels in large-scale challenges and effectively addresses optimization issues in solar mirror array layouts, showcasing its superior performance and stability across various applications.

Pisani et al. [8] presented a novel approach for optimizing the field of multi-tower heliostats using quantum computers, solving complex optimization problems that are challenging for conventional computational methods through quantum annealing. This innovative application of quantum computing to heliostat field optimization offers a new paradigm. Regarding algorithm development, Reddy et al. [9] used the derivative logarithmic sigmoid-woodpecker mating algorithm (DLS-WMA). They optimized an artificial neural network (O-ANN) to combine a cogeneration power plant with solar photovoltaic power generation in an industrial distribution system. The methodology aims to achieve a cost-effective and efficient system design to improve the efficiency of cogeneration power plants. Yadav et al. [10] conducted a comparative analysis of bionic algorithms for tracking the Global Maximum Power Point (GMPP) of PV systems under standard conditions, step changes in irradiance, and partial shadowing conditions.

Haris et al. [11] applied genetic algorithms to optimize the reflector field layout of solar thermal power plants, aiming to enhance the efficiency of central receiver solar thermal plants. Wang et al. [12] discussed the collaborative optimization of the mirror field and receiver in centralized solar power plants, aiming to improve system performance and reduce costs. Wang et al. [13] explored real-time targeting strategy optimization for the solar tower mirror field, proposing an enhanced particle swarm optimization (PSO) algorithm that treats mirrors as intelligent agents and incorporates a group inheritance mechanism to boost the algorithm's real-time efficacy.

Xie et al. [14] enhanced the Grey Wolf optimization algorithm by improving the convergence factor and weight updating formula, effectively mitigating local optima issues. Current research has focused on large-scale heliostat fields, but there is a considerable research gap in small-scale heliostats.

This paper explores ways to optimize energy production for maximum power output. It also proposes new models and layout optimization strategies for small-scale heliostat fields, supporting sustainable development goals. The contributions of this study are as follows:

(1) The layout of the traditional heliostat field is improved to enhance the power generation efficiency of the heliostat field.

(2) The dung-beetle optimization algorithm is improved by introducing the unique strategies of random walk and lateral movement, which enhances the search capability and adaptability of the algorithm in solving complex problems; the improved algorithm is then combined with the new layout of the heliostat field, which further enhances the power generation efficiency of the heliostat field. Then, the improved algorithm is combined with the new layout of the heliostat mirror field to further improve the power generation efficiency of the field.

(3) To verify the proposed scheme's accuracy, simulation experiments are carried out with MATLAB and compared with cutting-edge optimization algorithms, such as SSA, POA, DBO, etc. The results show that the RCDBO algorithm not only outperforms the other algorithms in the benchmark function test but also has a better performance in the power generation efficiency of the heliostat mirror field.

2. Mathematical modeling

In this part, the first part begins with a thorough description of the problem faced to ensure an accurate understanding of the problem. Next, Part II provides a detailed description of the parameters in the mathematical model. These parameters include not only the key variables that directly affect the solution of the problem but also those parameters that are ancillary

and provide additional information. Finally, Part III constructs a mathematical model that provides an in-depth analysis of the problem using mathematical tools and methods. The model enables the simulation of the actual scenario of the problem, predicts possible outcomes, and provides a basis for decision-making.

2.1. Problem description

Heliostat is a critical component of tower power stations, consisting of a mirror and a tracking system. Its size, height, quantity, and position significantly influence the optical and thermal efficiency of the heliostat field, subsequently impacting the power station's economy. Thus, the optimal design of the fixed sun mirror field is a crucial research area for tower power stations to maximize the annual average output thermal power per unit mirror area. To attain this objective, the focus is on the heliostats within a specific area of the heliostat field. There exists a complex interplay among the installation height h_j, position (x_j, y_j), and other parameters. The challenge lies in the layout planning, which must be strategically executed to optimize the performance of the heliostat field. A schematic diagram depicting the operational mechanism of the heliostat field has been constructed and presented in Fig. 1 to elucidate the principles of power generation within a heliostat field.

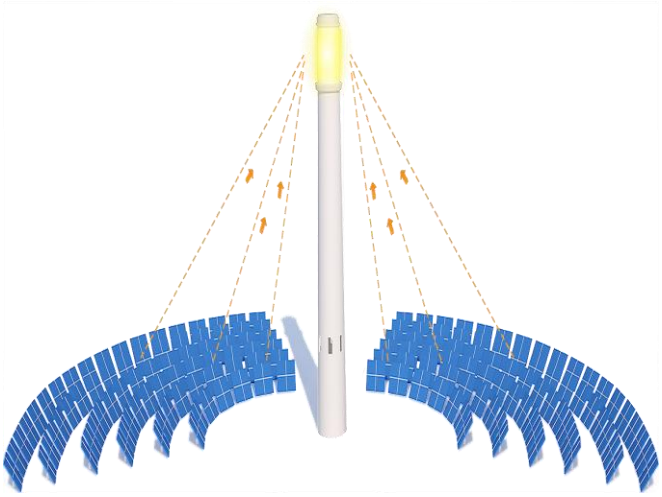

Fig. 1

2.2. Symbol specification

In the mathematical modeling section of this study, a tabular format is used to detail the critical parameters in the model. This presentation not only improves the readability of the information but also facilitates the reader to quickly grasp the core features of each parameter. The table lists the name and definition of each parameter and their specific role in the model. The details are shown in Table 1:

Table 1 Symbol Explanation Table

Parameter	implication
m_{ij}	Let m_{ij} be variable 0-1, when m_{ij} indicates that a heliostat with height type j is installed at position i, otherwise, no installation is required.
i	Represents all positions in the heliostats field coordinate system
j	The number of the heliostats
LH	Represents the side length of a rectangular heliostat.
LW	Represents the side width of a rectangular heliostat.
S	Represents the area of the heliostat; $S = LW \times LH$
DH	Represents the diameter of the circle of rotation trajectory of the rectangular heliostat; $DH = \sqrt{LW^2 + LH^2}$
R	Represents the radius of the installation range of the ring heliostat field;

2.3. Model assumption

(1) Determination of position: Select the center of the heliostat field as the position coordinate of the absorption tower and the coordinate origin of the three-dimensional coordinate system. The north, east, and upward are positive (the positive direction of the x-axis represents the north), and the position and installation height of the heliostats are indicated by the coordinate method. Unit: m.

(2) It is assumed that the heliostats encircle the collector in a circular arrangement.

(3) Since the heliostats were constructed in an arid climate zone, the impact of weather has been temporarily disregarded in the analysis.

2.4. Mathematical model representation

Considering the layout optimization model of the heliostat field, the power model is introduced, which is utilized to calculate the annual average thermal output power of the heliostat field. This calculation serves as the evaluation standard for the design of the heliostat field. Additionally, an optimization model for the heliostat field layout has been established to enhance the performance benefits of the heliostat field.

Annual average thermal output power $\overline{E_{field}}$ calculation model:

Due to variations in time and across seasons, changes in the sun's position result in alterations to the sun's azimuth and altitude angles. Consequently, the mathematical representation is as follows:

$$\overline{E_{field}} = \frac{\sum_0^{year} \int_{sunrise}^{sunset} E_{field}(x, y, h, t)dt}{T_{all}} \tag{1}$$

The Equation, T_{all} represents the total time, and the upper and lower limits of the integration represent sunrise time and sunset time, respectively.

2.4.1. The output thermal power of the heliostats field

$$E_{field} = DNI * \sum_{j}^{N} S_j \eta_j (x_j, y_j, h_j, t) * m_{ij}^u \tag{2}$$

$$DNI = G_0 \left[a + b \exp\left(-\frac{c}{\sin \alpha_s} \right) \right] \tag{3}$$

Where G_0 is the solar constant and its value is $1.366 KW / m^2$, H is the altitude (unit: km), a , b , c are the relevant constants, and the solar altitude angle α_s stands for Solar Altitude Angle, which is the angle between the sun's rays at a given location and the surface tangent that passes through the location and connects it to the earth's center. More information about a , b , c and $\sin \alpha_s$ can be found in the references [14]

DNI is the irradiance of normal direct radiation. It has been mathematically characterized as shown in the formula (3); N is the total number of heliostats(Unit: count); S_j is the lighting area of the j heliostats (unit: m^2); η_j is the optical efficiency of the mirror j .

Normal direct radiation irradiance DNI calculation model:

Normal direct radiation irradiance DNI refers to the solar radiation energy per unit area and per unit time in the plane perpendicular to the sun's rays on the Earth. For its verification and detailed information, see reference [14]:

The calculation model of the instantaneous optical efficiency η of heliostats has been proposed and verified in [15].

$$\eta = \eta_{sb}\eta_{\cos}\eta_{at}\eta_{trunc}\eta_{ref} \tag{4}$$

Where stands for shadow occlusion efficiency; $\eta_{\cos}$ stands for cosine efficiency; η_{at} represents the atmospheric transmittance; η_{trunc} represents the collector truncation efficiency, which is calculated using the HFLCAL model; η_{ref} stands for specular reflectivity, where η_{ref} is determined by the mirror material and can be seen as a constant, the value in this experiment is 0.92. The mathematical representations for these efficiencies are provided in the following equations.

2.4.2. Shadow occlusion efficiency model

Due to the varying heights of some heliostats. The fact that the frames of two adjacent heliostats are not parallel in actual conditions at the same solar altitude angle, the projections of the shading and blocking areas are not parallel either. This study employed the oblique projection method to determine the shadow occlusion efficiency η_{sb} between the mirrors accurately. Detailed information about the method's characterization and verification can be found in reference [11].

2.4.3 Cosine efficiency calculation model

According to the law of reflection, the cosine factor consists of the product between the incident solar unit vector and the heliostat normal unit vector, which is mathematically characterized as follows:

$$\eta_{\cos} = \cos(\theta) = \vec{S} \cdot \vec{N} \tag{5}$$

Where θ represents the incident Angle between the solar unit vector $\vec{S}$ and the normal unit vector; for details on the mathematical formulation, see [14-20].

2.4.4. Atmospheric transmittance model

This paper adopts an atmospheric attenuation efficiency model with a visibility of 40 km in clear weather, which was proposed and verified in [15-17]. Its mathematical representation is as follows:

$$\eta_{at} = \begin{cases} 0.99321 - 0.0001176 d_{HR} + 1.97 d_{HR}^2 & , (d_{HR} \le 1000m) \\ \exp(-0.0001106 d_{HR}) & , (d_{HR} > 1000m) \end{cases} \tag{6}$$

Where d_{HR} represents the distance from heliostats to the collector.

2.4.5. Collector truncation efficiency model

The HFLCAL model is a convolution model widely used to estimate truncation efficiency. The HFLCAL model is used to calculate the interception efficiency. In the HFLCAL model, the flux distribution of the heliometer located within the receiver boundary can be integrated to obtain the intercepted power fraction, which is commonly used to calculate the truncation efficiency. Detailed information on specific characterization and validation can be found in reference [16].

$$\eta_{trunc} = \frac{1}{2\pi\sigma_{tot}^2} \iint \exp\left(-\frac{x^2+y^2}{2\sigma_{tot}^2}\right) dxdy \tag{7}$$

Where, σ_{tot} represents the total dispersion of the flux distribution, which is calculated as follows:

$$\sigma_{tot} = \sqrt{d_{HR}{}^2(\sigma_{sun}^2 + \sigma_{bq}^2 + \sigma_{ast}^2 + \sigma_{tract}^2)} \tag{8}$$

The Equation, σ_{sun} represents the shape of the sun, σ_{bq} represents the beam quality error caused by the slope error of the mirror, σ_{ast} represents the astigmatism effect, and σ_{track} represents the tracking error;

$$\sigma_{bq} = \left(2\sigma_{slope}\right)^2 \tag{9}$$

$$\sigma_{ast} = \frac{\sqrt{0.5\left(H_t^2 + W_s^2\right)}}{4d_{HR}} \tag{10}$$

Where, σ_{slope} represents the slope error of the mirror surface, H_t represents the size of the light spot on the collector in the numerical direction, and W_s represents the size of the light spot on the collector in the horizontal direction. For more information about the HFLCAL model, please refer to references [16-17].

2. 5. Layout optimization model:

Objective function: Since the heliostat field can convert the collected thermal energy into electrical energy, which in turn can serve more industries, this paper uses the maximum annual average thermal output power $\max \overline{E_{field}}$ as a criterion to assess the efficacy of the heliostat field design. Therefore, this paper establishes an objective function to maximize this parameter to reflect the optimization of the design for thermal performance.

Constraint condition:

(1) Due to the challenges in converging reflected light within 100 meters around the collector and the limited scope of the heliostat field, the number and coordinates of the heliostats installed require specific attention. Consequently, the constraints are defined to accommodate these particularities in the installation parameters:

$$\sum_j m_{ij}^u = N, \forall i \in I; \tag{11}$$

$$100 \le \sqrt{x_j^2 + y_j^2} \le 350 \tag{12}$$

$$\sqrt{x_j^2 + y_j^2} \le R \tag{13}$$

(2) To ensure that the heliostats do not touch the ground when rotating, specific measures were implemented; the installation height of the mirror must be greater than half of the width of the mirror.

$$h > \frac{1}{2}LW \tag{14}$$

$$\sqrt{\left(x_a - x_b\right)^2 + \left(y_a - y_b\right)^2} > \frac{1}{2}DH_a + \frac{1}{2}DH_b + 5, a, b \in j \tag{15}$$

In addition, to ensure the cleaning and maintenance of the mirror, the distance between the heliostats and the heliostats must be greater than 5 m; In formula (15).

(3) To ensure uniform installation heights for the heliostats on each ring, the following restriction is applied:

$$\begin{cases} d_{HRa} = d_{HRb} \\ s.th_a = h_b \end{cases} \tag{16}$$

$$\begin{cases} d_{HRa} < d_{HRc} \\ s.t.h_a < h_c \end{cases} \tag{17}$$

3. Random walk and cross dung beetle optimization algorithm.

Dung Beetle Optimizer (DBO) is a new swarm intelligence optimization algorithm proposed by Xue et al. in 2022. [18]. The algorithm is inspired by the rolling, dancing, foraging, stealing, and breeding behaviors of dung beetles. In the algorithm, the position of each dung beetle represents a solution to the problem, and the position of the optimal dung beetle is the optimal solution to the problem being solved. Because of its relatively simple algorithmic structure and good performance, it has been successfully applied to optimization problems in many fields, but it still needs to be improved. For example, the solution accuracy needs to be improved, the convergence speed is slow, and the local optimum is not jumped out in the late iteration. Therefore, to address the above problems, this paper proposes the dung beetle optimization algorithm with random wandering and vertical and horizontal crossover.

3.1. The crossbar strategy disturbed the ball-rolling behavior of dung beetles

As the first stage behavior of the dung beetle algorithm, the rolling behavior of the dung beetle determines the optimization ability of the whole algorithm by searching the global position. In this improvement, a random walk strategy was adopted to carry out a disturbance at the stage of dung beetle ball rolling behavior [19]. In order not to increase the algorithm's complexity, it is set that when the optimal value of the dung beetle algorithm does not change during the five iterations, the random walk strategy is adopted.

The random walk strategy formula is as follows:

$$X(t) = \left\{0, c_{\text{ussum}}\left[2r(t_1)-1\right], c_{\text{ussum}}\left[2r(t_2)-1\right], \cdots, c_{\text{ussum}}\left[2r(t_n)-1\right]\right. \tag{18}$$

Take a random function $r(t)$ as follows:

$$r(t) = \begin{cases} 1, \text{rand} > 0.5 \\ 0, \text{rand},, 0.5 \end{cases} \tag{19}$$

Because the trajectory of the intelligent algorithm has a specific range, it cannot update the position of the algorithm directly with the above formula. It needs to be normalized to ensure that the algorithm walks within a certain range, as shown in the following equation.

$$X_i^t = \frac{(X_i^t - a_i)(d_i^t - c_i^t)}{(b_i - a_i)} + c_i^t \tag{20}$$

In the formula, X_i^t represents the position of the i-th dung beetle in the t-th iteration; a_i and b_i are the minimum and maximum values of the i-th dimensional random walk variable, respectively; c_i^t and d_i^t are the minimum and maximum values of the i-th dimensional random walk variable in the t-th iteration, respectively.

3.2. The crossbar strategy disturbed the ball-rolling behavior of dung beetles

The strategy of cross and cross includes horizontal cross and vertical cross. The blind spots can be reduced and the algorithm has a better global search ability when the population is searched by horizontal cross. The premature convergence of most population intelligent search algorithms is caused by some stagnant dimensions of the population. Vertical crossing can promote some stagnant dimensions of the population to get rid of premature convergence so that the algorithm can jump out of the local optimal. Meanwhile, the operation of crossing can increase the diversity of the population. The cross-cutting strategy also involves a competitive process in which the resulting children are compared with their parents to ensure that the updates are made in a better direction. Horizontal and vertical crosses are carried out successively, and the two crosses influence each other to improve the algorithm's solving accuracy and accelerate the convergence speed. The following is a brief introduction to these two cross-operations.

Horizontal crossing is an arithmetic crossing that operates on all dimensions between two different individuals. Individuals in the population are randomly matched first, then the paired individuals are randomly matched, and then the two paired individuals are crossed laterally. Suppose that SM_{i1} and SM_{i2} are paired paternal individuals, with their children representing SM_{i1}^{hc} and SM_{i2}^{hc}, resulting from the following mathematical representations:

$$SM_{i1j}^{hc} = r_1 \cdot SM_{i1j} + (1-r_1) \times SM_{i2j} + c_1 \cdot (SM_{i1j} - SM_{i2j}) \tag{21}$$

$$SM_{i2j}^{hc} = r_2 \cdot SM_{i2j} + (1-r_2) \cdot SM_{i1j} + c_2 \cdot (SM_{i2j} - SM_{i1j}) \tag{22}$$

$$SM_{ij1}^{vc} = r \cdot SM_{ij1} + (1-r) \cdot SM_{ij2} \tag{23}$$

Where SM_{i1j} and SM_{i2j} represent the j th dimension of SM_{i1} and SM_{i2}, respectively, $j = 1,2,\cdots,D$, SM_{i1j}^{hc} and SM_{i2j}^{hc} are the j th dimensions where SM_{i1j} and SM_{i2j} cross horizontally to produce children on the j th dimension, respectively. r_1 and r_2 are uniformly distributed random numbers in the $(0,1)$ range, while c_1 and c_2 are uniformly distributed random numbers in the $(-1,1)$ range. The resulting progeny are compared with its Parent generation separately, preserving the individual with a smaller objective function value. Vertical crossover is the dimensional arithmetic crossing of all individuals on two different dimensional operations. Each individual performs a longitudinal crossover to update only one of the dimensions, leaving the other dimensions unchanged, providing a plan for the stagnant dimension to jump out of the local optimal without destroying another possible optimal dimension. Assuming vertical crossover, two dimensions j_1 and j_2 are randomly selected, and the j_1 th dimension of its Offspring SM_i^{vc} is given by Eq. (23), while the other dimensions remain consistent with the parent SM_i.

Among them, r is a uniformly distributed random number within the $(0,1)$ range. Compare the generated offspring with their parents and retain individuals with smaller objective function values. The vertical and horizontal cross strategy is applied at the end of the dung beetle algorithm to perturb the entire population. To avoid increasing algorithm complexity, this improvement introduces a cross-strategy factor pv, which is mathematically represented as follows:

$$pv = \frac{2 \times (1 - (b/M)^{1.5})}{3} \tag{24}$$

Among them, b represents the current number of iterations, and M represents the total number of iterations. When $r > pv$, the vertical and horizontal crossing strategy is adopted, and when $r < pv$, the vertical and horizontal crossing strategy is skipped in this iteration. Here is the pseudo-code for the RCDBO algorithm:

Algorithm RCDBO Algorithm

Input: *pop, M, c, d, dim, fobj*
Output: *fMin, bestX, Convergence curve, Trajectories, fitness history, position history*
Initialize parameters and bounds
Initialize population *x* using chaos mapping
for each individual *i* in population **do**
    Calculate fitness *fit*(*i*) = *fobj*(*x*(*i*, :))
end for
Set *pFit* = *fit*, *pX* = *x*, *XX* = *pX*
Find global optimum *fMin* and *bestX*
for each iteration *t* from 1 to *M* **do**
    Record historical data
    Determine *worse*, *r*2, *RB*, *min c*, *max d*
    for each producer *i* **do**
        if *t* > 5 and convergence curve unchanged **then**
            Apply random walk strategy
        else
            Update position using original strategy
        end if
        Apply bounds and calculate fitness
    end for
    Find current optimum *fMMin* and *bestXX*
    Update positions *Xnew*1, *Xnew*2, *Xnew*11, *Xnew*22
    for each non-producer *i* **do**
        Update position using respective equations
        Apply bounds and calculate fitness
    end for
    Update global best positions and finesses
    if random probability > *pv* **then**
        for each individual *i* in population **do**
            Apply horizontal and vertical crossover strategies
        end for
    end if
    Record convergence curve
    end for
    Function: Apply bounds

3.3. Feasibility analysis of random walk and cross-dung beetle optimization algorithm

In this study, the algorithm is evaluated using several high-dimensional test functions and is compared with new optimization algorithms, including Dung Beetle Optimization (DBO), Sparrow Search Algorithm (SSA), and Pelican Optimization Algorithm (POA), to validate the optimization performance of the Random Walk and Crossbar Dung Beetle Optimization Algorithm (RCDBO). Where the parameters Dung Beetle Optimization Algorithm (DBO) have a proportion of rolling dung beetles of 0.2, a proportion of brood balls of 0.2, a proportion of dung beetle hatchlings of 0.25, and a proportion of stealing dung beetles of 0.35; Sparrow Search Algorithm (SSA) has a parameter warning value of 0.6, a proportion of finders of 0.7, and a proportion of those who are aware of being by a hazardous sparrow of 0.2; and the parameter constant R in Pelican Optimization Algorithm (POA) has a parameter constant of 0.2;

Several typical CEC-Benchmark functions are selected to assess the enhanced results of the RCDBO algorithm. The benchmark function test set is documented in reference [21]. The population size of the algorithm is set to 30, with a maximum of 500 iterations. Each algorithm, combined with the test functions, was independently executed 30 times to record the optimal values, average values, and standard deviations of the test function results, which are detailed in Tables 2 through 6.

Table 2 Results of the test function f_1

Test function	Algorithm	Optimal value	Average value	Standard deviation
f_1	RCDBO	0.0000	0.0000	0.0000
	DBO	2.0659×10^{-159}	4.3729×10^{-112}	2.3952×10^{-111}
	SSA	5.4505×10^{-113}	2.2692×10^{-49}	1.2429×10^{-48}
	POA	1.6599×10^{-119}	1.0499×10^{-103}	3.9202×10^{-103}

Table 3 Results of the test function f_2

Test function	Algorithm	Optimal value	Average value	Standard deviation
f_2	RCDBO	0.0000	0.0000	0.0000
	DBO	9.4745×10^{-80}	6.1809×10^{-58}	3.3852×10^{-57}
	SSA	0.0000	1.2190×10^{-31}	4.3667×10^{-31}
	POA	2.7574×10^{-59}	5.2632×10^{-51}	2.5455×10^{-50}

Table 4 Results of the test function f_6

Test function	Algorithm	Optimal value	Average value	Standard deviation
f_6	RCDBO	2.8828×10^{-07}	1.6879	6.4228
	DBO	25.0725	25.7796	0.30474
	SSA	3.1019×10^{-09}	7.9753×10^{-05}	3.88411×10^{-4}
	POA	26.7304	28.1180	0.6964

Table 5 Results of the test function f_7

Test function	Algorithm	Optimal value	Average value	Standard deviation
f_7	RCDBO	0.0000	0.0000	0.0000
	DBO	9.1194×10^{-06}	0.0050	0.0245
	SSA	1.1904×10^{-16}	0.0002	0.0001
	POA	1.3499	2.7444	0.6083

Table 6 Results of the test function f_9

Test function	Algorithm	Optimal value	Average value	Standard deviation
f_9	RCDBO	0.0000	0.0000	0.0000
	DBO	5.6211×10^{-125}	2.4222×10^{-28}	9.2163×10^{-28}
	SSA	0.0000	1.6661×10^{-17}	7.2842×10^{-17}
	POA	3.0633×10^{-116}	1.5152×10^{-101}	6.3485×10^{-101}

It can be seen from the above table that the comprehensive optimization ability of the RCDBO algorithm is relatively better. For the optimal solution of the test function f_1, f_2, f_6, f_7, f_9, the accuracy of the RCDBO algorithm is significantly higher than that of the other two algorithms. Regarding mean value and standard deviation, the RCDBO algorithm is several orders of magnitude higher than other algorithms. For f_9 function, although the RCDBO algorithm is consistent with the optimal value of the SSA algorithm in the final numerical accuracy, its optimization process is faster than the SSA algorithm. The RCDBO algorithm has better optimization and stability according to the above results.

4. Simulation experiment

The simulation experiments in this study are divided into two phases, firstly to verify the feasibility of the model and secondly to demonstrate the effectiveness of the improved algorithm in solving the model. In the first phase, through scientific and systematic experimental design, we verified the applicability and effectiveness of the model in simulating a specific phenomenon, providing an empirical basis for the model. In the second phase, through a series of experiments, we tested and demonstrated the advantages of the improved algorithm in increasing the solving efficiency and optimizing the results while maintaining the solving accuracy. The experimental results of these two phases not only confirm the practicality of the model and algorithm but also provide a solid foundation for future research and applications.

4.1 Model validation

The computational approach of this model was utilized within MATLAB to optimize the heliostat field located at the Nujiang (28.38° N, 98.65° E) in Yunnan Province to determine the maximal average annual heat output power achievable. Table 7 presents the critical parameters for configuring the computational model, alongside the environmental characteristics of the region and details regarding the heliostat field.

Simulation experiments were conducted using MATLAB to validate the practical applicability of the proposed model to engineering problems. The process involves two stages: initially, the planar position (x_j, y_j) of the entire heliostat field is ascertained. Subsequently, the Dung Beetle Optimization (DBO) algorithm is employed to solve two variants of the heliostat field model. The conventional variant assumes a uniform mounting height h for all heliostats, while the novel variant allows for differing mounting heights for some heliostats. The objective is to compute the maximum annual average heat output power $\overline{E_{field}}$. The outcomes of these simulation experiments are presented in Table 8:

Table 7 Details of experimental parameters

Parameter	Value	Unit	Parameter	Value	Unit
x_j	$100 \le x_j \le 350$	m	H	1526	m
y_j	$100 \le y_j \le 350$	m	N	2104	count
h_j	$2 \le h_j \le 5$	m	LH	5.5	m
h_T	84	m	LW	5.5	m
h_r	8	m	σ_{sun}	2.51	$mrad$
x_T	0	m	σ_{track}	0.63	$mrad$
y_T	0	m	σ_{bq}	0.89	$mrad$

Table 8 Improved before-and-after comparison data tables

parameter	Before improvement	After improvement
$\overline{E_{field}}$	$3.8995\times10^4 MW$	$4.0124\times10^4 MW$
η_j	0.62230	0.64033
η_{sb}	0.9512	0.9638
$\eta_{\cos}$	0.6865	0.6968
η_{trunc}	0.9892	0.9897
η_{at}	0.9634	0.9634

The simulation experiment data, as delineated in Table 8, reveal that the newly developed model has demonstrated marked improvements in parameters η_{sb}, $\eta_{\cos}$, and η_{trunc} when juxtaposed with the traditional heliostat field model. This comparison presupposes that the two heliostat fields have the same plane position (x_j, y_j) of the heliostats they contain at the time the comparison is made. The enhancement in parameters is especially notable, with a more significant improvement compared to parameters $\eta_{\cos}$ and η_{trunc}. This substantial improvement is predominantly due to the innovative feature of the model, which includes using varied mounting heights for specific heliostats, thereby effectively reducing the incidence of shadow occlusion. The identical plane position (x_j, y_j) in both models results in a consistent value for η_{at} derived from each model. The new model has notably achieved an approximate 2% increase in the average annual heat output. These results not only affirm the viability and superiority of the proposed model but also open up possibilities for further improvements in the heat output efficiency of heliostat mirror fields, marking a significant step forward in the field of solar energy concentration.

4.2 Model solving

Utilizing the relevant parameters outlined in Table 7, the proposed model was simulated and solved using advanced optimization algorithms, including RCDBO, DBO, SSA, and POA. The resulting experimental data are presented in Table 9, Fig. 2, and Fig. 3.

Table 9 Comparison data of various algorithms

parameter	Before improvement	After improvement
$\overline{E_{field}}$	$3.8995\times10^4 MW$	$4.0124\times10^4 MW$
η_j	0.62230	0.64033
η_{sb}	0.9512	0.9638
$\eta_{\cos}$	0.6865	0.6968
η_{trunc}	0.9892	0.9897
η_{at}	0.9634	0.9634

Upon comparing the data in Table 9 and Fig. 3, it is readily apparent that the improved dung beetle algorithm (RCDBO) outperforms the dung beetle optimization algorithm (DBO), the sparrow algorithm (SSA), and the pelican algorithm (POA) in terms of total instantaneous time integration efficiency and various efficiencies of the proposed heliostat mirror field model. This substantiates that the RCDBO algorithm exhibits superior optimality and stability in optimizing the heliostat mirror field. Moreover, Fig. 2 clearly illustrates that the average annual heat output power computed by the RCDBO algorithm significantly surpasses that of other algorithms. Regarding specific data, the annual average heat output power $\overline{E_{field}}$ computed by RCDBO is approximately 3% higher than that of the preceding algorithm and about 2% higher than that of the other two optimization algorithms. These data demonstrate the feasibility of the RCDBO algorithm in solving the new model of the heliostat mirror field, a result that holds considerable significance for research and application in the field of solar energy.

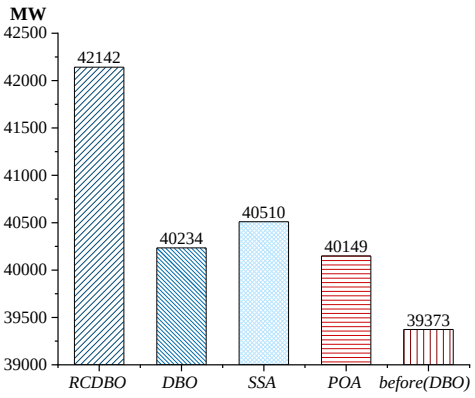

Fig. 2 Efficiency contrast bar chart

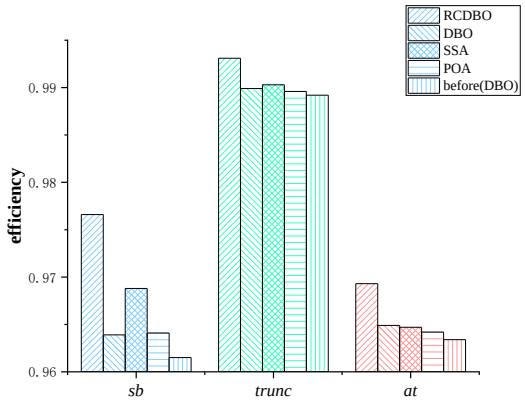

Fig. 3 Efficiency histogram

The dung beetle algorithm will be Improved (RCDBO) to depict the layout pattern of the proposed model and the efficiency distribution within the heliostat field more effectively. Utilizing the data derived from this solution, all heliostats throughout the entire field will be ranked based on their efficiency. Their equivalent circles will then be color-coded to construct an efficiency contour map, as depicted in Fig. 4. Furthermore, a detailed view of the high-efficiency zones averaged annually within the heliostat field will be presented, as shown in Fig. 5.

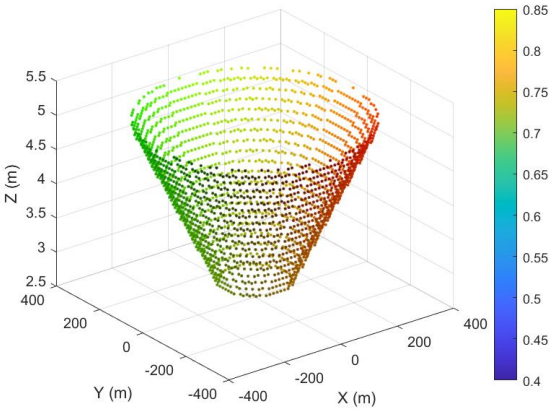

Fig. 4 Layout efficiency contour

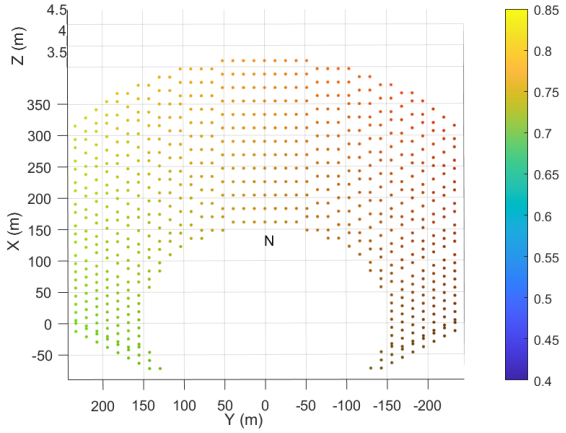

Fig. 5 Partial view of the high-efficiency area

Fig. 4 presents a three-dimensional depiction of the arrangement scheme for the newly introduced heliostat field. Fig. 5 reveals the localized distribution of the sectors that exhibit greater efficiency within the field. Considering that the simulation experiment is conducted north of the Tropic of Cancer, the heliostats located in the northern sector of the field receive a higher degree of solar exposure, which inherently results in superior performance in terms of efficiency when compared to those situated in the southern sector. As a result, the regions within the heliostat field that demonstrate high efficiency are predominantly concentrated in the northern area.

5. Conclusion

In this study, the problem of low power generation efficiency of the traditional heliostat field is considered, and the conventional heliostat field layout model is improved. This study introduces random wandering and vertical and horizontal crossover strategies and proposes an improved dung-beetle optimization algorithm (RCDBO). Additionally, the validity of the proposed model and algorithm is verified through the simulation experiments with accurate data.

This research results can be applied to the photovoltaic field, and the annual average thermal output power of the fixed-sun mirror field reaches 67% through the application in the Nujiang area. Although this study has improved the annual average heat output power. However, the study's limitations are that land utilization, construction costs, and operational costs still need to be considered. Future studies on fixed-heaven mirror fields should focus not only the efficiency improvement but also on the land use rate, construction costs, and operational costs to achieve greater economic benefits.

Acknowledgments

This work was supported by the Science and Technology Project of China Southern Power Grid Co., Ltd., under Grants YNKJXM20230530 and the National Key Research & Development Program of China under Grants 2023YFB2407300.

Conflicts of Interest

The authors declare no conflict of interest.

References

[1] N. C. Giri, S. Das, D. Pant, V. S. Bhadoria, D. P. Mishra, G. Mahalik, et al., “Access to Solar Energy for Livelihood Security in Odisha, India,” Signals, Machines, and Automation, Springer Nature, pp. 235-242, 2022.

[2] B. Wang, Y. Liu, D. Wang, C. Song, Z. Fu, and C. Zhang, “A Review of the Photothermal-Photovoltaic Energy Supply System for Building in Solar Energy Enrichment Zones,” Renewable and Sustainable Energy Reviews, vol. 191, article no. 114100, March 2024.

[3] N. C. Giri, K. K. Shah, S. S. Ray, H. Vennila, S. Das, Y. B. Sandhya, et al., "Photovoltaic Pumping System vs. Livelihoods and Sustainability," Ambient Science, vol. 9, no. 1, pp. 27-30, January 2022.
[4] T. Arrif, A. Sánchez-González, B. Bezza, and A. Belaid, "Shadowing and Blocking Factors in Heliostats: Comparison between Parallel and Oblique Projections," SOLARPACES 2020: 26th International Conference on Concentrating Solar Power and Chemical Energy Systems, AIP Publishing, vol. 2445, no. 1, article no. 120004, May 2022.
[5] B. Gao, H. Sun, and S. Liu, "Heliostat Field Layout Optimization of Solar Tower Power Station Based on Improved Whale Algorithm," Acta Energiae Solaris Sinica, no. 10, pp. 209-217, 2023.
[6] Y. Zou, Y. Zhou, and Q. Xu, "Heliostat Field Layout via Niching and Elite Competition Swarm Optimization," IEEE Access, vol. 12, pp. 31589-31604, 2024.
[7] T. Arrif, S. Hassani, M. Guermoui, A. Sánchez-González, R. A. Taylor, and A. Belaid, "GA-GOA Hybrid Algorithm and Comparative Study of Different Metaheuristic Population-Based Algorithms for Solar Tower Heliostat Field Design," Renewable Energy, vol. 192, pp. 745-758, June 2022.
[8] L. Pisani, G. S. Moreau, E. Leonardi, C. Podda, A. Mameli, and G. Cao, "Multi-tower Heliostat Field Optimization by Means of Adiabatic Quantum Computer," Solar Energy, vol. 263, article no. 111893, October 2023.
[9] B. K. Reddy, N. C. Giri, P. K. Yemula, E. B. Agyekum, and Y. Arya, "Optimal Operation of Cogeneration Power Plant Integrated with Solar Photovoltaics Using DLS-WMA and ANN," International Journal of Energy Research, vol. 2024, no. 1, article no. 5562804, 2024.
[10] D. Yadav, N. Singh, N. C. Giri, V. S. Bhadoria, and S. K. Sarker, "Comparison of Bioinspired Techniques for Tracking Maximum Power under Variable Environmental Conditions," International Journal of Intelligent Systems, vol. 2024, no. 1, article no. 6678384, 2024.
[11] M. Haris, A.U. Rehman, S. Iqbal, S. O. Athar, H. Kotb, K. M. Aboras, et al., "Genetic Algorithm Optimization of Heliostat Field Layout for the Design of a Central Receiver Solar Thermal Power Plant," Heliyon, vol. 9, no. 11, article no. e21488, November 2023.
[12] Y. Wang and D. Ni, "Real-Time Aiming Strategy Optimization of Heliostat Field of Solar Power Tower via a Modified PSO Algorithm (SPSO)," 2023 China Automation Congress (CAC), IEEE, pp. 368-373, 2023.
[13] S. Wang, C.-A. Asselineau, A. Fontalvo, Y. Wang, W. Logie, J. Pye, et al., "Co-optimization of the Heliostat Field and Receiver for Concentrated Solar Power Plants," Applied Energy, vol. 348, article no. 121513, October 2023.
[14] Q. Xie, Z. Guo, D. Liu, Z. Chen, Z. Shen, and X. Wang, "Optimization of Heliostat Field Distribution Based on Improved Gray Wolf Optimization Algorithm," Renewable Energy, vol. 176, pp. 447-458, October 2021.
[15] R. Conceição, A. M. Hernández, M. Romero, and J. González-Aguilar, "Experimental Soiling Assessment, Characterization and Modelling of a Highly-Compact Heliostat Field in an Urban Environment," Solar Energy, vol. 262, article no. 111812, September 2023.
[16] K. Xu, H. Xu, and J. Fan, "Research on Optimization Model Based on Heliostat Field," Highlights in Science, Engineering and Technology, vol. 82, pp. 99-107, 2024.
[17] H. Li, R. Zhang, C. Liu, and J. Yin, "Optimized Design of Heliostat Field Efficiency Based on Finite Element Analysis Method," Proceedings of 2024 IEEE 3rd International Conference on Electrical. Engineering, Big Data Algorithms (EEBDA), IEEE, pp. 1371-1376, 2024.
[18] J. Xue and B. Shen, "Dung Beetle Optimizer: A New Meta-Heuristic Algorithm for Global Optimization," The Journal of Supercomputing, vol. 79, no. 7, pp. 7305-7336, May 2023.
[19] M. Guermoui, T. Arrif, A. Belaid, S. Hassani, N. Bailek, "Enhancing Direct Normal Solar Irradiation Forecasting for Heliostat Field Applications Through a Novel Hybrid Model," Energy Conversion and Management, vol. 304, article no. 118189, March 2024.
[20] I. Paul and S. B. Kedare, "Determination of Optically Feasible Heliostat Field Region for Solar Power Tower System Employing Innovative Receiver Aperture," Solar Energy, vol. 271, article no. 112404, March 2024.
[21] F. A. Hashim, E. H. Houssein, K. Hussain, M. S. Mabrouk, and W. Al-Atabany, "Honey Badger Algorithm: New metaheuristic algorithm for solving optimization problems," Mathematics and Computers in Simulation, vol. 192, pp. 84-110, February 2022.